JOURNAL OF GEOPHYSICAL RESEARCH, VOL. 115, C01002, doi:10.1029/2009JC005381, 2010

Atmospheric methane flux from bubbling seeps: Spatially extrapolated quantification from a Black Sea shelf area

Jens Greinert,[1,2] Daniel F. McGinnis,[3] Lieven Naudts,[1] Peter Linke,[3] and Marc De Batist[1]

Received 13 March 2009; revised 1 October 2009; accepted 7 October 2009; published 12 January 2010.

[1] Bubble transport of methane from shallow seep sites in the Black Sea west of the Crimea Peninsula between 70 and 112 m water depth has been studied by extrapolation of results gained through different hydroacoustic methods and direct sampling. Ship-based hydroacoustic echo sounders can locate bubble releasing seep sites very precisely and facilitate their correlation with geological or other features at the seafloor. Here, the backscatter strength of a multibeam system was integrated with single-beam data to estimate the amount of seeps/m^2 for different backscatter intensities, resulting in 2709 vents in total. Direct flux measurements by submersible revealed methane fluxes from individual vents of 0.32–0.85 l/min or 14.5–37.8 mmol/min at ambient pressure and temperature conditions. A conservative estimate of 30 mmol/min per site was used to estimate the flux into the water to be 1219–1355 mmol/s. The flux to the atmosphere was calculated by applying a bubble dissolution model taking release depth, temperature, gas composition, and bubble size spectra into account. The flux into the atmosphere (3930–4533 mol/d) or into the mixed layer (6186–6899 mol/d) from the 21.8 km^2 large study area is three times higher than independently measured fluxes of dissolved methane for the same area using geochemical methods (1030–2495 mol/d). The amount of methane dissolving in the mixed layer is 2256–2366 mol/d. This close match shows that the hydroacoustic approach for extrapolating the number of seeps/m^2 and the applied bubble dissolution model are suitable to extrapolate methane fluxes over larger areas.

Citation: Greinert, J., D. F. McGinnis, L. Naudts, P. Linke, and M. De Batist (2010), Atmospheric methane flux from bubbling seeps: Spatially extrapolated quantification from a Black Sea shelf area, *J. Geophys. Res.*, *115*, C01002, doi:10.1029/2009JC005381.

1. Introduction

[2] Fluxes of free and dissolved methane at cold seep sites have a strong impact on the local carbon cycle. The occurrence of free gas (bubbles) in the sediment and in the water column results from local methane supersaturation under the ambient temperature and pressure conditions [*Boudreau et al.*, 2001], and a sediment methane reservoir sustaining this supersaturation.

[3] Because free methane in the sediment cannot directly be consumed by microbes (i.e., through anaerobic oxidation of methane (AOM) or aerobic methane oxidation), it bypasses these very effective microbial filters [*Boetius and Suess*, 2004; *Sommer et al.*, 2006] and is released into the bottom water as bubbles. As a bubble rises, the gas composition in the bubble constantly changes as methane dissolves and oxygen, nitrogen and other gases are stripped from the water [*Leifer and Patro*, 2002; *McGinnis et al.*, 2006; *Holzner et al.*, 2008]. If the initial bubble is large enough and the water is rather shallow (<100 m), some of the methane will be released into the atmosphere [*McGinnis et al.*, 2006].

[4] The amount of methane released by natural gas seeps into the water column and into the atmosphere is highly variable and remains, despite several attempts of quantification, largely unknown, even for small, well-studied areas [*Hovland et al.*, 1993; *Hornafius et al.*, 1999; *Dimitrov*, 2002b; *Etiope and Klusman*, 2002; *Etiope*, 2004; *Judd*, 2004; *Kvenvolden and Rogers*, 2005; *Luyendyk et al.*, 2005; *Bange*, 2006; *Kessler et al.*, 2006]. Current estimates of global methane fluxes from the seabed to the atmosphere vary by over 2 orders of magnitude between 0.4 and 48 Tg yr^{-1} [*Judd*, 2004]. The main obstacle for establishing reliable estimates for regional and global methane flux is the spatial and temporal variability of seep activity and intensity.

[5] Here, we present a new approach to quantify the methane flux from cold seeps, which takes into account the spatial and temporal variability of the seepage and a numerical model for methane dissolution into the seawater during bubble rise. It is based on (1) single-beam echo sounder data for bubbling seep detection and mapping; (2) multibeam backscatter data for the extrapolation of the total number of seeps in different depth intervals of the study area; (3) direct bubble flux measurements by a submersible; (4) lander-based high-resolution monitoring of the temporal variability of bubble release; and (5) application of a bubble dissolution model to estimate the amount of

[1]Renard Centre of Marine Geology, Ghent University, Ghent, Belgium.
[2]Royal Netherlands Institute for Sea Research, Den Berg, Netherlands.
[3]Leibniz Institute of Marine Science, IFM-GEOMAR, Kiel, Germany.

0148-0227/10/2009JC005381$09.00

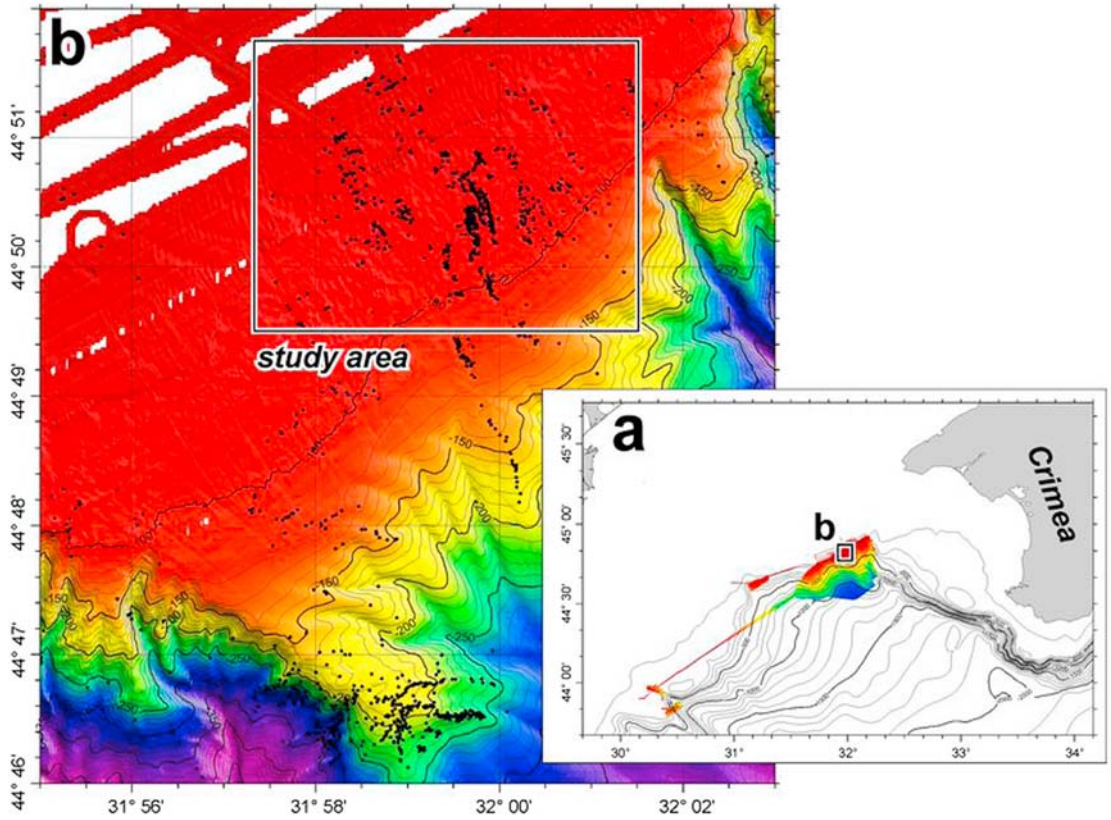

Figure 1. (a) Regional bathymetry map of the area mapped in 2003 and 2004 during the CRIMEA and METROL projects in the Black Sea, west of the Crimea Peninsula. (b) Enlarged map of the Dnepr Paleo Delta area showing the hydroacoustically mapped bubble release spots (black dots) and the study area. The contour interval is 10 m.

methane that is transported to the sea surface or into to the mixed layer. The combination of these techniques provides a novel and systematic approach to estimate methane flux which is compared to other geochemically and hydroacoustically determined fluxes.

2. Study Area

[6] The presented data were recorded during two cruises in 2003 and 2004 within the framework of the European Commission-funded Contribution of High-Intensity Gas Seeps in the Black Sea to Methane Emission to the Atmosphere (CRIMEA) project at the continental shelf and slope in the NW Black Sea. The region lies 130 km west of the Crimea Peninsula, off the mouth of the Dnepr River (Figure 1) and is characterized by a great abundance of clustered bubble-releasing seeps [*Egorov et al.*, 2003; *Naudts et al.*, 2006] known to have been active for more than 10 years [e.g., *Egorov et al.*, 1998].

[7] Seaward of the shelf edge, at about 105 m water depth, the seafloor dips gently with a 0.55° slope to the SE and is incised by canyons (Figures 1b and 2). A terrace-like ridge between 180 and 250 m water depth shows a very dense accumulation of bubble seeps, that were the focus of several studies between 2001 and 2004 [e.g., *Michaelis et al.*, 2002; *Schmale et al.*, 2005; *Naudts et al.*, 2006]. The main study area of this paper is on the shelf between 70 and 112 m (Figure 1) with the most active seep area between 85 and 95 m water depth [*Naudts et al.*, 2008].

[8] *Naudts et al.* [2006] described more than 2000 bubbling seeps and correlated them to morphological and subsurface features such as ridges, pockmarks, sediment slides, shallow gas and gas-hydrate-induced bottom-simulating reflectors (BSRs). They also showed that a 3 to 4 m deep, acoustically detected gas front in the subsurface typically shallows at areas of intense clustering of bubbling seeps.

[9] With a water depth of ~70 m, the shallowest parts of the study area are still within the oxygen-rich euphotic zone. The rest lies in the oxycline between 80 and 115 m, where the oxygen concentration drops from 285 to 10 μM at the top of the suboxic layer [*Oguz*, 2002]. Oxygen is completely absent below 145 m, the uppermost layer of the anoxic zone in the Black Sea.

[10] The dense clusters of seeps in the study area show a direct relationship between seep-released methane, surface water methane concentration, and methane flux into the atmosphere [*Schmale et al.*, 2005]. Surface water methane concentrations were about 2 to 2.5 times higher (up to 7.5 nM) than the "normal" shelf or open water concentrations in the Black Sea (4.5 and 3 nM, respectively).

3. Methods

[11] In this study different hydroacoustic methods and data sets were merged to define the seep-influenced area, to

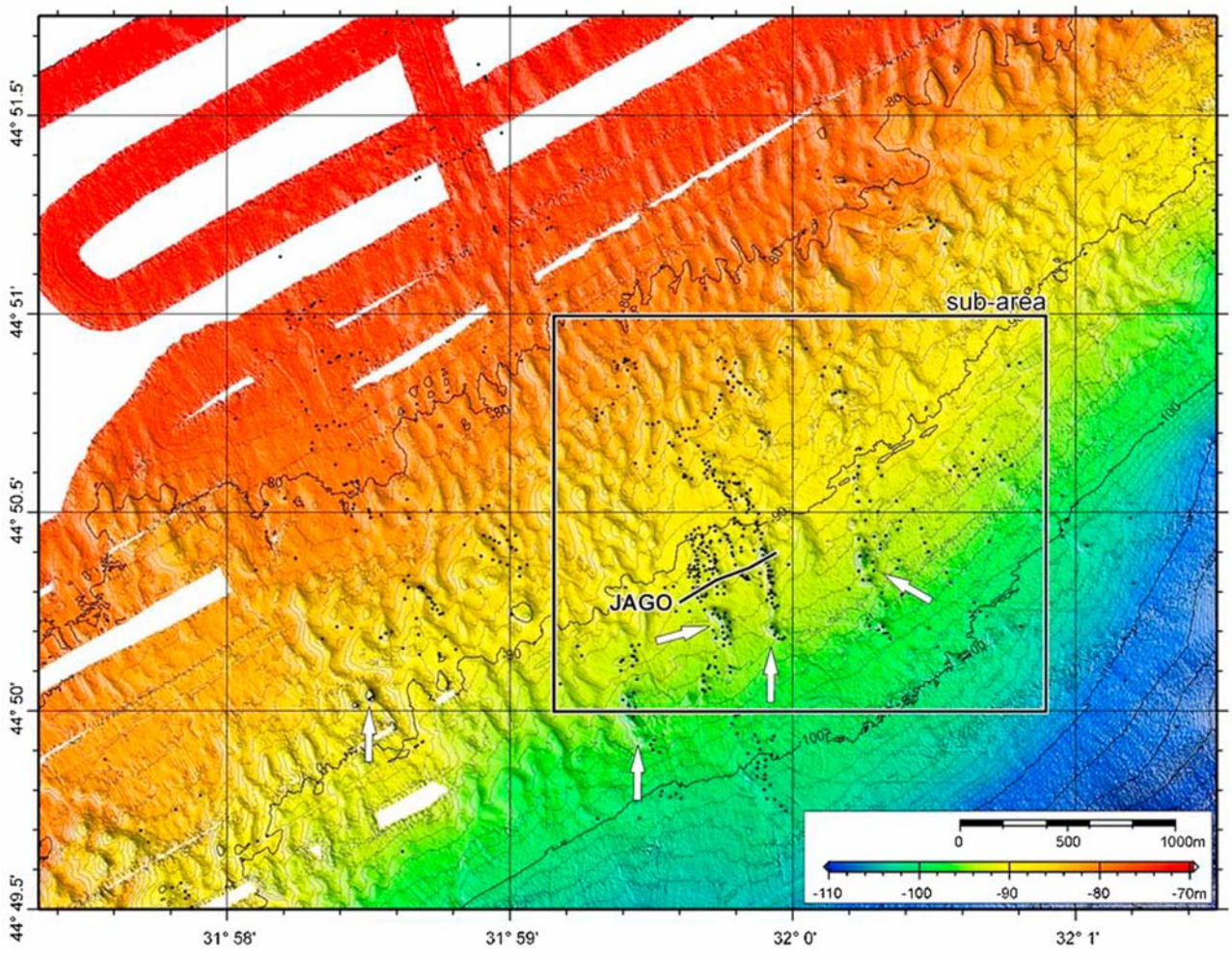

Figure 2. Bathymetric map of the study area showing the wave-like structured shelf and the shelf edge toward the SE. Black dots represent bubble seeps detected during the two CRIMEA cruises in 2003 and 2004 (n = 645). The rectangle defines the subarea used for the correlation between seeps/m^2 and backscatter values (see text). White arrows point to pockmarks. The line labeled JAGO shows the dive track during which direct flux measurements and seafloor observations have been done (Figure 7). The contour interval is 1 m; illumination from the NE.

establish a relationship between backscatter values and the density/number of seeps and finally to estimate the number of seeps for specific depth intervals. The data acquisition and processing techniques are described in this section. The integration and analysis of the data sets are described in section 5.

3.1. Bubble Detection and Mapping by Single-Beam Echo Sounder

[12] Bubbles in the water column can be easily detected using echo sounder systems due to the strong acoustic impedance difference between water and free gas. We used the hull-mounted scientific single-beam echo sounder EK500 on the RV *Prof. Vodyanitskiy* to detect, map, monitor and analyze bubbles as they rose in the water column [*Artemov*, 2006; *Artemov et al.*, 2007]. The backscattered signal of the dual frequency split beam system (120 and 38 kHz) was continuously recorded digitally, providing an enormous database for later digital analyses. The single-beam echo sounder coverage was dense but did not cover the entire study area completely.

[13] Postprocessing of the data used the WaveLens software package [*Artemov*, 2006]. The location of bubble releasing seeps was identified by picking the positions of flare-shaped backscatter signals in echograms, which are caused by bubbles in the water column (thus the term "flare imaging" used for these surveys). As the EK500 system provides the position of single targets (e.g., fish or bubbles) within the main lobe of the acoustic beam, it is possible to calculate the real target strength of bubbles and, because of the relationship between bubble size/pressure and target strength, determine their in situ size and how it changes during rise (assuming spherical bubbles).

[14] Some of the data were recorded during very calm sea conditions when the ship was at anchor above bubble-releasing spots. This allowed the bubble-release activity to be monitored over a long time (i.e., up to several hours) and flux estimates of free gas from the bubble-releasing site to

be made [*Artemov et al.*, 2007]. Calibration of the EK500 system followed the method described by *Anon* [1991]. See *Artemov* [2006] for a detailed description of the WaveLens software and the applied analytical methods.

3.2. Bathymetry and Backscatter Mapping by Multibeam Echo Sounder

[15] Multibeam echo sounders typically provide water depth values (x-y-z data), and modern multibeam systems also record the strength of the backscattered signal that is detected as seafloor. We used a Seabeam 1050 system that is capable of recording the backscatter data. The system has 50 kHz transducers and was custom installed on RV Professor Vodyanitskiy as a 120° swath system, transmitting and receiving 126 focused beams with a beam angle of 3° by 3°. Multibeam recording was carried simultaneously with seismic and flare-imaging single-beam surveys at an average survey speed of 4 to 6 knots.

[16] Multibeam data were recorded with the Hydrostar Online software of L3 Communications ELAC Nautik. The data were preedited with HDPEdit and converted to x-y-z data with HDPPost (L3 Communications ELAC Nautik) prior to 3D fine editing with Fledermaus (Interactive Visualization Systems). The raw backscatter data (bottom amplitude values) were corrected for incidence angle with HDPPost assuming a flat seafloor. Data were exported from HDPPost and spikes were removed with Fledermaus. HDPPost normalizes the backscatter values and they do not represent "real" dB values but unscaled backscatter units (BU).

3.3. Data Visualization, Area Calculation, and Processing

[17] GMT 4.2.1 was used for data visualization and the area calculation of different backscatter values using the *grdvolume* command [*Wessel and Smith*, 1998]. Distance calculations between seeps and high-backscatter areas were performed with ESRI ArcGIS 9.1.

3.4. Bubble-Release Monitoring With GasQuant

[18] Bubble release from the seafloor is a highly intermittent process that changes over short (minutes to hours) and long time scales (hours to years). In most of the reported cases, bubble release changes on a minute to daily basis and can be triggered by phenomenon such as tides or waves [*Dimitrov*, 2002a; *Leifer and MacDonald*, 2003; *Sauter et al.*, 2006; *Greinert et al.*, 2006; *Greinert*, 2008; *Schneider et al.*, 2009]. To monitor this transient behavior, the hydroacoustic lander system GasQuant was deployed in the study area for 55 h in June 2004 [*Greinert*, 2008]. The GasQuant system can monitor an area of 2075 m^2 with high temporal (4 s) and spatial resolution. The horizontally looking multibeam swath consists of 21 beams with 3° beam angle. Each beam is sampled in 10 cm cells, which results in 10752 cells that are monitored simultaneously. A detailed description of the system, the applied processing steps, and a detailed discussion of the results are given by *Greinert* [2008].

3.5. Direct Bubble Flux Measurements and Bubble Observations

[19] Several dives with the submersible JAGO observed and sampled bubble-releasing spots in the study area. In addition to the 92 m deep study area described here, bubble sampling was also undertaken at a 250 m deep site [*Michaelis et al.*, 2002]. An inverse funnel was used to capture bubbles and directly sample the gas upon release from three different seeps. The funnel was attached to a glass cylinder with volumetric marks to allow flux calculations. These measurements were performed six to seven times at each of the three seeps.

[20] On board, the collected gas was transferred into 20 ml headspace vials for compositional and isotopic analyses. The vials were stored upside down with 4 ml of NaCl-saturated water as a barrier against gas exchange.

[21] Digital video recording from inside the submersible through the large front window was used to determine bubble size distributions. The dives were part of the studies undertaken within the European Commission-funded project Methane Flux Control in Ocean Margin Sediments (METROL; MPI-Bremen, Germany).

4. Results

4.1. Bathymetry, Seafloor Backscatter, and Seep Occurrence

[22] Multibeam mapping reveals a gently southeastward sloping shelf between 70 and 105 m water depth (Figure 2). Two types of features characterize the shelf morphology. Most dominant are sediment waves that strike around 140° with 70 to 120 m wavelength and amplitudes of 50 to 120 cm. The origin of these sediment waves is not clear. They may have been formed rather recently by water currents, but probably represent remnants of a dune field developed during the last glacial lowstand. Pockmarks are the second characteristic morphological feature. They are between 60 and 90 m in width with a depth of less than 2.5 m. Single pockmarks often merge to form larger, elongated features that can reach up to 600 m in length. These features are mainly oriented N–S.

[23] As discussed by *Naudts et al.* [2006], the occurrence of bubbling seeps in the study area is closely linked to the up doming of a subsurface gas front, often in or close to the elongated pockmarks. A multibeam backscatter map shows that seeps almost exclusively occur in or very close to irregularly shaped areas of high backscatter (Figure 3). This high backscatter is not related to the medium-intensity backscatter pattern of the dune morphology. We therefore used these irregularly shaped high-backscatter patches as an indicator for seepage and the spatial extrapolation of the amount of seeps in the area.

[24] Only some parts of the dune areas have backscatter values similar to those of the seep-indicating patches (Figure 3). Those backscatter values typically occur on the eastern flanks of the dunes (Figure 4) as stretched oval-shaped patches that are repeated rather regularly in E–W direction. The density of seeps does not increase in these areas (Figure 3).

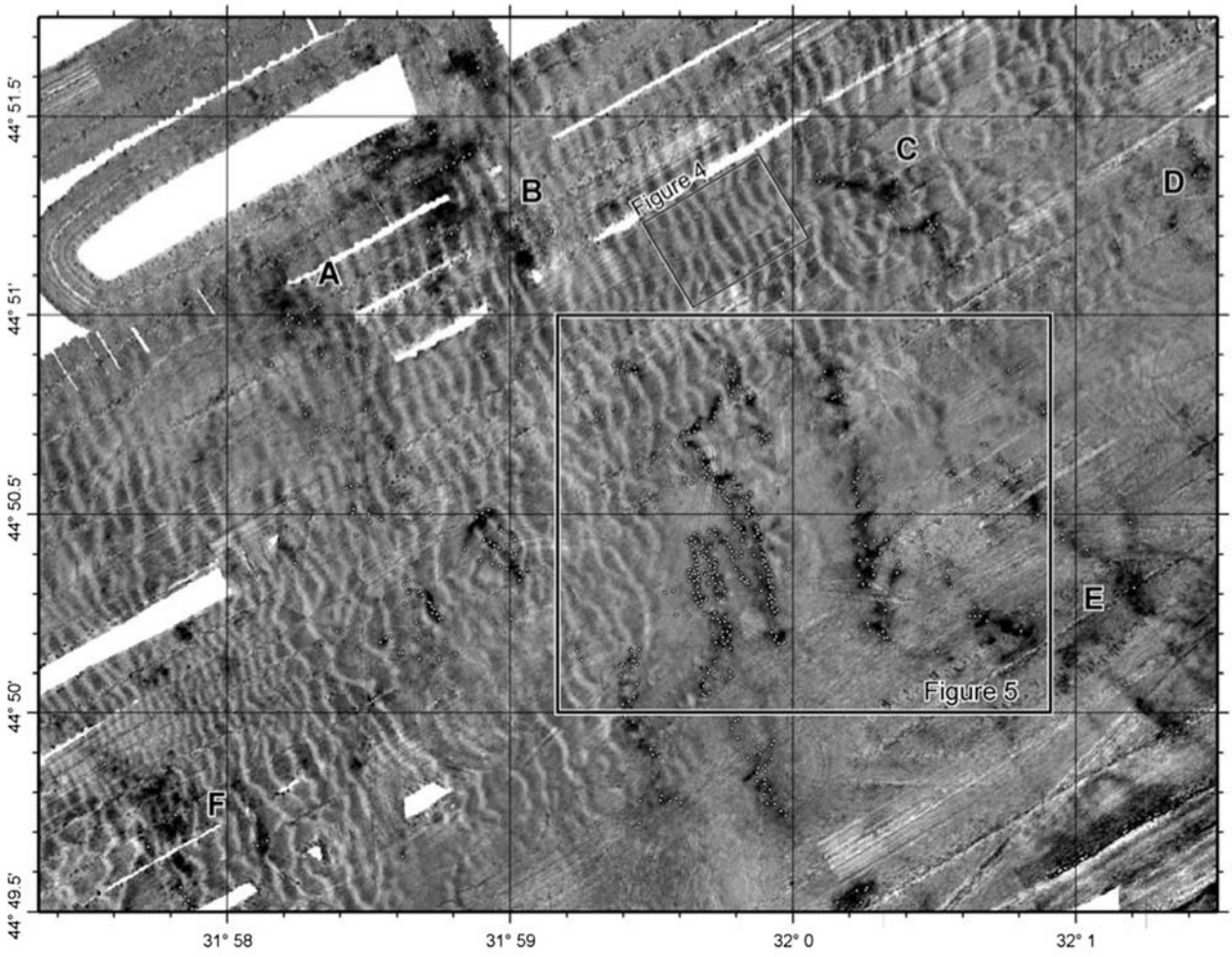

Figure 3. Backscatter map of the study area. The wave-like pattern striking NNW–SSE are clearly visible as well as patches of very high backscatter (black), which fit well with the observed seep sites (little white dots). Areas A–F are different high-backscatter areas. The subarea used for getting the relation between backscatter intensity and seeps/m^2 is outlined by a rectangle and shown enlarged in Figure 5.

[25] The single-beam echo sounder coverage shows survey artifacts and as a result only a few seeps were identified within the three northern high-backscatter patches (areas A–C) and within those east and west of the central seep cluster (areas D–F in Figure 3). To minimize this survey artifact and to establish a statistically significant relationship between seep occurrence and areas of different backscatter values (the seep density per m^2 for specific high-backscatter values), a smaller subarea was chosen to have a more detailed and denser coverage of seeps detected by the single-beam echo sounder (Figure 5).

[26] For visualization purposes and later spatial extrapolation, the backscatter value at each seep site was extracted and plotted as histogram and sum curve (Figure 6). None of the 645 seeps of the entire study area occurs where backscatter values are below −4.5 BU; the distribution is Gaussian with a mean of 1.52 and a median of 1.78. The same is true for the subarea with 382 seep sites (Figure 6). Different colors are used to highlight specific backscatter ranges (Figures 5 and 6). They were chosen based on how many seeps (75, 50, 25 and 5%) plot into the area with equal or higher-backscatter values. 75% of all seeps plot in areas of ≥0.47 BU (this equals 20% of the subarea in Figure 5a), 50% plot in ≥1.75 BU (7.2% of subarea), 25% in ≥3 BU (1.7% of subarea) and 5% in ≥4.75 BU (0.6% of subarea). The 5% range was specifically defined because such high values almost exclusively occur within the seep-related high-backscatter patches and is used to exclude nonseep areas during the process of extrapolating the total number of seeps in the study area (section 5.1.2).

[27] Figure 5a shows the subarea using the same color code as for Figure 6. Figure 5b covers the same subarea, but shows only those parts that have been covered at least once with the single-beam echo sounder. Comparing image A and B shows that one reason for the apparent nonoccurrence of seeps in the high-backscatter areas at the eastern part of the subarea is the lack of single-beam data. However, there are very high-backscatter areas ≥4.75 BU in which no seeps

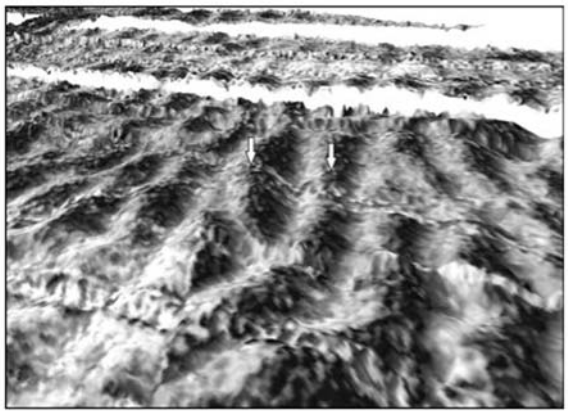

Figure 4. Three-dimensional view (toward NNW) of the backscatter map draped over bathymetry between the high-backscatter areas B and C (see Figure 3). The elevated backscatter related to the dunes typically occurs at their eastern side. The distance between the two arrows is 105 m (wavelength); the wave amplitude is 1.2 m. The image only shows the backscatter map draped over the bathymetry; no illumination is applied.

were found despite sufficient single-beam coverage. Two conclusions seem possible, either no seeps exist in those areas or the seeps were not active during the single-beam survey. Both possibilities and their implications are discussed below.

4.2. Seafloor Observations and Direct Flux Measurements

[28] Direct visual seafloor observations during a JAGO dive in the study area (Figure 7) showed a rough (micro-relief in cm) but generally flat seafloor with very little relief on dm scale. The sediment surface is typically composed of shell fragments in a sand to silt matrix of brownish to gray color (Figure 7). Bright white bacterial mats occur as irregularly shaped patches of dm^2 to m^2 size. They were found either as single patches or in large clusters covering tens of m^2. Bubbles were released either from within bacterial mats, from their edges or from between bacterial mats when they occurred in larger clusters. Detailed observations at bacterial mats sometimes showed that gas was first captured in a reservoir just below the mat surface (up doming of the mat) before it was released as a "single bubble" or in the form of "bubble streams" (i.e., bubbles released one after another at a more or less constant rate). Bubble streams were common in contrast to more vigorously bubbling holes, which released several bubbles at the same time forming a column of rising bubbles ("bubble columns").

[29] Bubble columns show a greater range of bubble sizes, with more small bubbles than in bubble streams or solitary bubbles. The overall size range was 2 mm to 16 mm in diameter. Bubbles 6–7 mm in diameter were very common and large bubbles were only occasionally observed. Sampling with push cores revealed that the sediment below bacterial mats is often very hard. This changed to softer sediment a few centimeters away from the mat. Digging with the submersible claw below mats frequently exposed solid carbonate chunks or little crusts; digging sometimes also failed because the substratum was too hard.

[30] In addition to these visual observations, three direct bubble flux measurements were performed at different locations in the subarea. The fluxes varied between 0.55 and 1.44 ml/s (Table 1) with the highest fluxes measured by trapping a bubble column (several bubbles released at the same time; up to 36 bubbles s^{-1}). The two other measurements were made at relatively constant bubble streams that released only one bubble at a time.

5. Discussion

[31] To estimate the amount of free gas released from the seafloor into the water column, into the mixed layer, and to the sea over the entire area, several processing steps are needed. First, the total number of seeps for the entire area has to be determined by extrapolating the observed relationship between seep occurrence and acoustic backscatter values. Second, the average of direct flux measurements has to be multiplied by the number of seeps to provide the total methane flux from the seafloor into the water column. Third, the amount of gas transported to the sea surface or into the mixed layer is calculated using a gas bubble dissolution model, considering the release depth, bubble size spectra and gas composition. Finally, knowing the number of seeps in a certain water depth allows estimating the total flux of methane from the seafloor to the sea surface or into the mixed layer.

5.1. Extrapolating the Total Number of Seeps

5.1.1. Calculating Seep Density

[32] To calculate how many seeps exist in the entire study area, we established a correlation between backscatter value and the number of acoustically detected seeps per m^2 that "typically" occur in the area with the respective backscatter value. As this correlation is based on those seeps that were detected by the single-beam echo sounder, only the area that was actually insonified by the system in the small subarea (Figure 5b) was considered for establishing a correlation. The number of seeps in a certain backscatter range (from ≤ -4.0 to ≥ 6.25 BU in 0.25 intervals) was divided by the respective areas to get the number of seeps per m^2.

[33] Two linear correlations can clearly be seen in Figure 8b. There is only a slight increase in seeps/m^2 with increasing backscatter for values below 0.25 BU, while significantly more seeps/m^2 can be found in areas with increasing backscatter values between 0.5 and 2.5 BU. For areas above 2.5 BU, the number of seeps/m^2 is highly variable but the trend increases slightly with increasing backscatter values.

[34] This variability may be due to the reduction in seafloor area with increasing backscatter values and the inaccuracy of locating the bubble releasing spot at the seafloor (submeter scale) and the footprint size of the multibeam and gridding artifacts (meter scale). Thus it might happen that a seep position might lie just outside a high-backscatter area although it actually lies inside, and vice versa. Another possibility is that the number of seeps/m^2 is indeed very variable. *Naudts et al.* [2008] attribute this

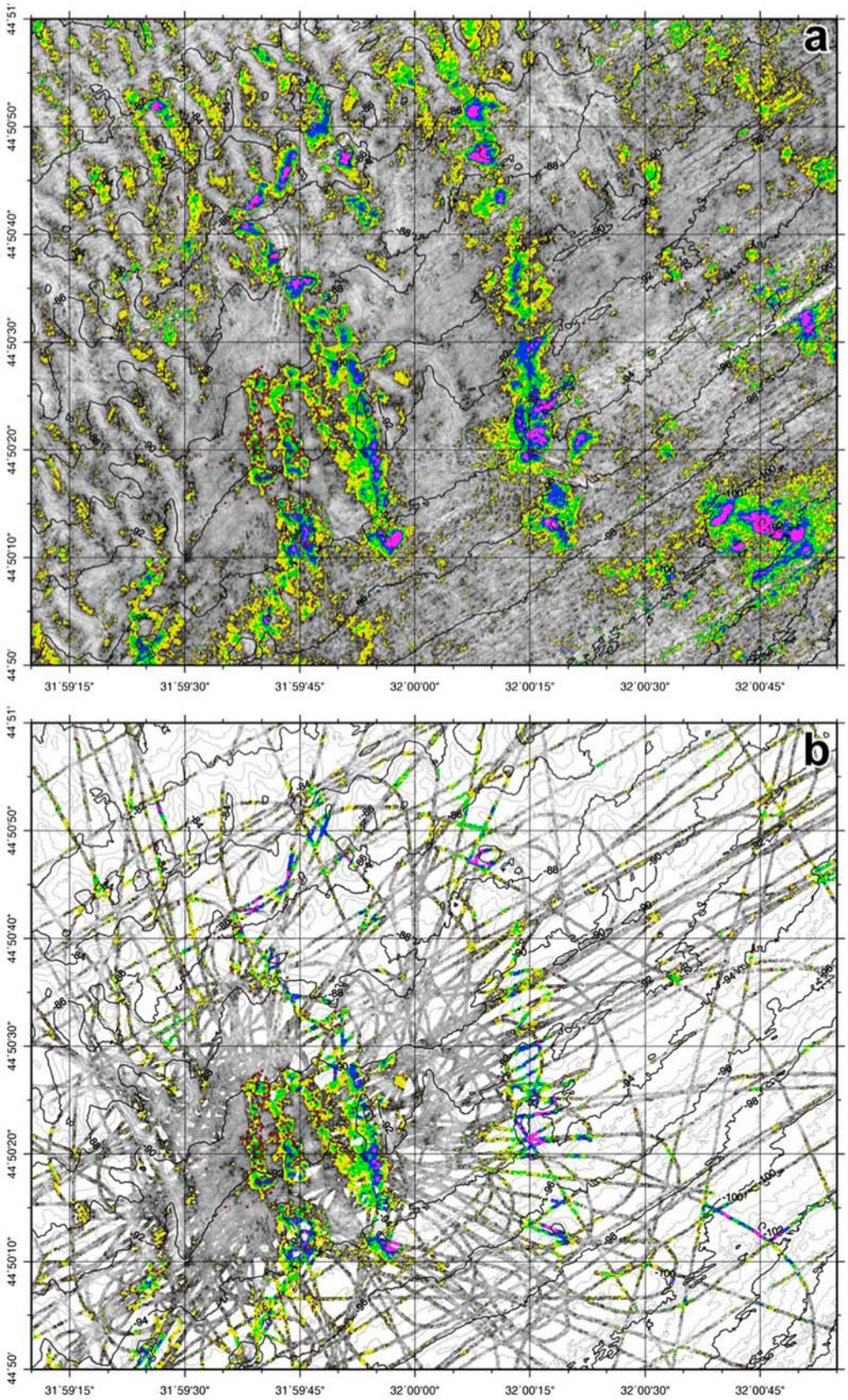
a
b
44°51'
44°50'50"
44°50'40"
44°50'30"
44°50'20"
44°50'10"
44°50'
31°59'15"
31°59'30"
31°59'45"
32°00'00"
32°00'15"
32°00'30"
32°00'45"

Figure 5

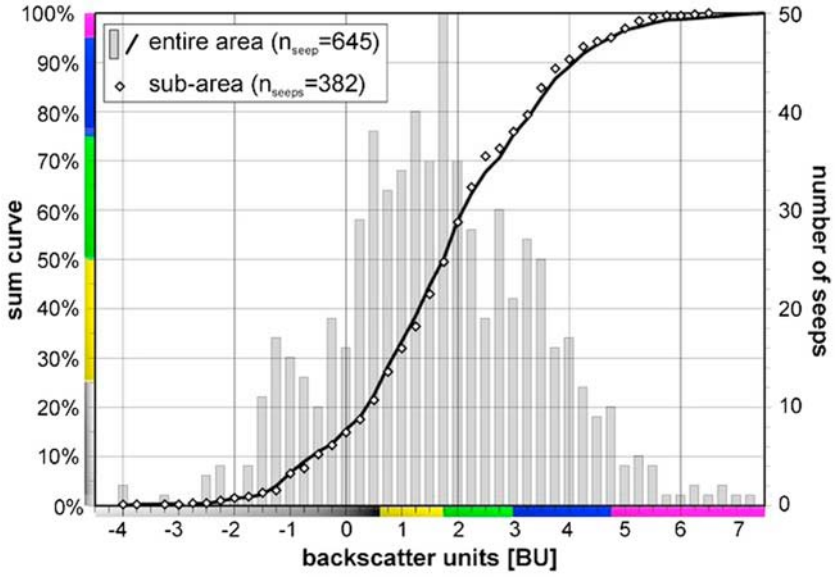

Figure 6. The distribution of backscatter values at seep positions clearly indicates that most seeps occur in higher-backscatter areas (75% at values ≥0.47 BU equals 21% of the area). The color changes were set at 75, 50, 25, and 5% of seeps occurring in areas with backscatter values ≥0.47, 1.75, 3.0, and 4.75 BU, respectively.

variability to a process of self-sealing of seeps due to enhanced carbonate formation via AOM. This forces fluids to migrate around the carbonate barrier which results in bubble release away from the strongly cemented and strongly reflective areas.

5.1.2. Spatial Extrapolation of the Number of Seeps

[35] Before using the relationship between seep density and backscatter value for spatial extrapolation of the real number of seeps in the study area, the area considered for extrapolation has to be defined to exclude high-reflectivity areas that are not associated with seepage. The western flanks of the dunes, which have high-backscatter values most likely caused by sediment sorting, and high-backscatter artifacts on the steeper slope in the SE corner of the study area were excluded. The SE corner was cut off at the 120 m contour line (Figure 9b).

[36] It was found that 95% of all seeps occur within 80 m of backscatter values ≥4.75 BU (Figure 10). We suggest that this very high reflectivity is caused by AOM-derived carbonate cementation of the sediment that is strongest in the center of an actively methane seeping area. As backscatter values in the dune areas are mostly below 4.75 BU, most of the dune fields could be excluded (Figure 9c). Nevertheless, some dune areas remained that do not seem to be influenced by seepage but were not cut out because of high-backscatter spikes in the center part of the multibeam swath. These areas were manually excluded to reduce the possibility of overestimation (Figure 9d).

[37] Applying the ''seep density versus backscatter'' relationship of Figure 8b results in numbers of seeps for the different processing steps that range from 5085 to 2709 (Figure 9), with 2709 seeps being the most likely number in the study area. 645 seeps were detected by single-beam echo sounder, which suggests that only about 25% of all seeps were discovered during the intensive hydroacoustic surveying.

5.2. Flux Into the Water

[38] To calculate the overall free methane flux from the entire area into the water column, we used the number of seeps (=2709) extrapolated from the backscatter/seep relation multiplied by the averaged directly measured flux of 0.5 mmol/s. This sums up to 1.4 t/d of carbon (1354.5 mmol/s; Table 2).

[39] *Greinert* [2008] observed that only one of 17 seeps was active for 75% of the observation time in this area. On average, each seep was only active for 12%; some of them showed a very periodic bubble release cycle of a few hours, with, e.g., 1.2 min bubbling interrupted by a 7 min long pause. Applying a temporal correction of 12%, the flux of 1.4 t/d of carbon decreases to 168 kg/d (= 13996 mol/d CH_4). In relation to the entire area (21.8 km^2), this means that 7.7 mg/d/m^2 of carbon is released as methane; this is about the equivalent of the smoke of one cigarette. The appropriateness of a correction for the temporal variability is discussed in section 5.6.

Figure 5. Backscatter maps, color coded for different ranges of backscatter values (see Figure 6) from the subarea outlined in Figure 3. (a) Coverage of the multibeam system (4.25 km^2). (b) Area that was insonified with the single-beam echo sounder (10 m footprint). Only this area (1.65 km^2) was used to get the correlation between the number of seeps/m^2 and varying backscatter values (Figure 8). Sum curves of the different backscatter value areas are identical for the multibeam (Figure 5a) and single-beam (Figure 5b) map.

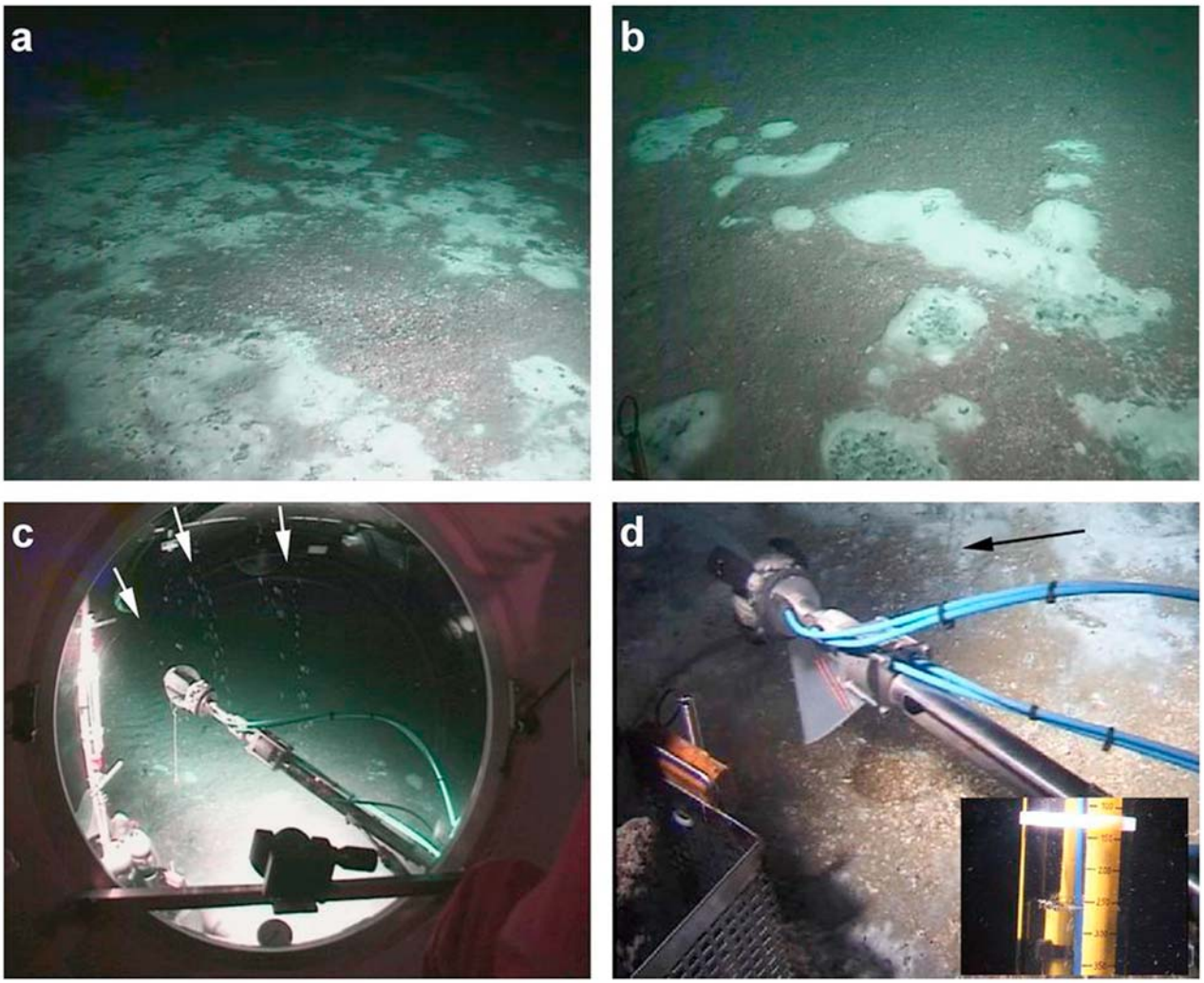

Figure 7. Seafloor images recorded during the submersible dives with JAGO in 2004. (a and b) The flat seafloor around seep sites is typically covered with white *Beggiatoa* mats. Bubbles are released from within the mats or very close to their outer edge. (c) Three bubble streams only a few tens of cm apart. The claw of the submersible holds a little metal sphere (6 mm in diameter) as scale for the bubble size. (d) The inverted funnel over a bubble stream during one of the flux measurements.

5.3. Gas Dissolution and Stripping During Bubble Rise

[40] Methane transport to the atmosphere strongly depends on how much methane is dissolved from the bubbles during their rise through the water column. Dissolution is controlled by the release water depth, the initial bubble size and the environmental conditions (Figure 11). *McGinnis et al.* [2006] presented a model for calculating the exchange of gases out of (dissolution) and into (stripping) rising bubbles. This model was modified and implemented into an easy to use GUI [*Greinert and McGinnis*, 2009], that allows calculating how much of the initially released methane (in bubble form) reaches the sea surface (in bubble form). Figure 12 shows how the gas composition and bubble sizes change for different initial bubble sizes and release depths.

[41] Because of the sensitivity of the response to these factors, it is crucial to subdivide the study area into depth intervals (<73 m; 73 to 112 m in 3m intervals) and to

Table 1. Directly Measured Bubble Fluxes in the Study Area and Some Examples From the Literature for Comparison

	Bubble Flux ml/s[b]	Bubble Flux l/min STP	CH_4 (mmol/min)
Measurements			
1	0.55	0.32	14.45
2	0.74	0.44	19.44
3	1.44	0.85	37.83
Average	0.91	0.57	23.91
Comparisons			
Hakon Mosby MV (1250 m)	23–50		7620–16,680
Hydrate Ridge (600 m)	16–83		2460–12,900
Batumi seep, Black Sea (850 m)	maximum of 92		20,280
Bulgarian shelf (5–22 m)[a]	6.6–58		24–215

[a]Here mmol/min is calculated for 15 m water depth and 20°C.
[b]In situ; 92 m water depth.

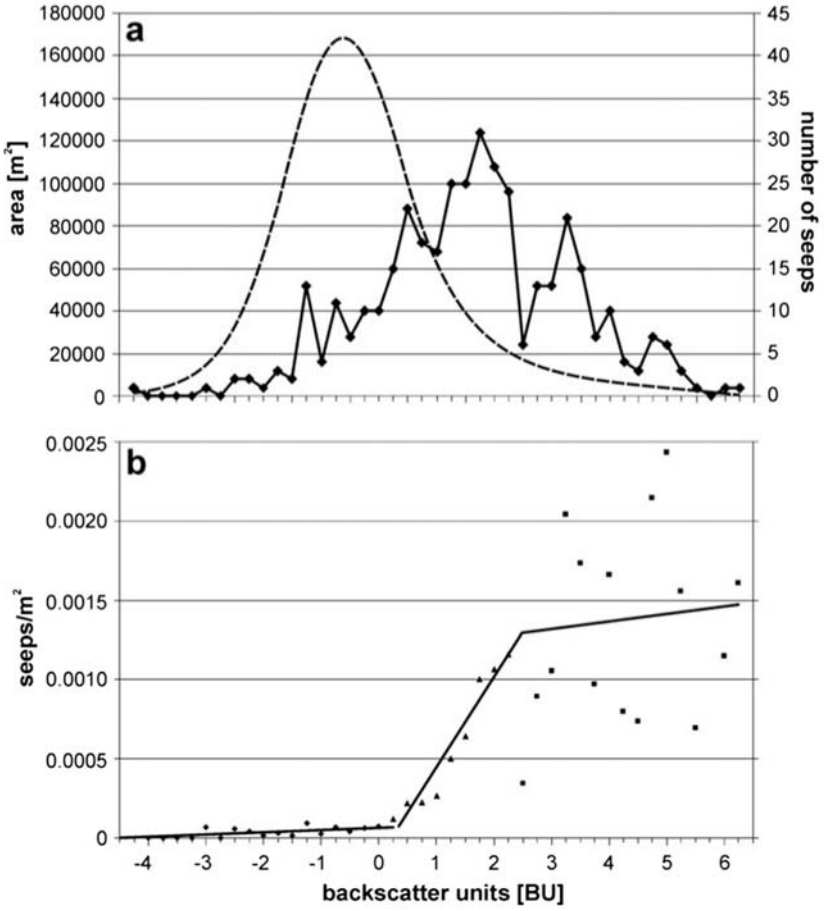

Figure 8. (a) The respective area (dashed line) for each of the defined backscatter ranges (0.25 wide) and the number of seeps (solid line and symbols). (b) A good correlation that can be described by three linear functions is clearly indicated. The scattering around the highest backscatter values is caused by an increasing error due to the smaller area and the additional temporal variability of seep activity.

assume the most probable bubble size spectrum to make a reasonable estimate of the percentage of methane transported to the sea surface. Based on the visual observations of the initial bubble sizes, the flux for four bubble-size distributions (Gaussian shaped) was calculated over the entire depth range for pure methane bubbles (Figure 13). The assumption of Gaussian distributed bubble sizes is supported by observations at the Vodyanitskii mud volcano in the Black Sea [*Sahling et al.*, 2009], that show a Gaussian distribution and a mean diameter of 5.2 mm.

[42] Model results show that, depending on the initial bubble size, the presence of small amounts of nitrogen (or other gases) in the initial bubble will increase the amount of methane that reaches the atmosphere. Figure 14 gives an example of how the final methane concentration of a 6, 8, 10 and 12 mm bubble changes if the initial methane concentration varies between 100 and 50%. The model predicts that the amount of methane transported to the sea surface increases in small bubbles, with increasing N_2 content for a 6 mm bubble, and reaches a maximum at 20% N_2 for an 8 mm bubble. The reason for this is the lower concentration difference between the bubble and the dissolved gases in the water if nitrogen is present in the bubble.

[43] As bubbles between 6 and 8 mm are the most common in our data set, it is very important to know the exact initial gas composition to improve our estimate of the methane flux to the atmosphere. *Schmale et al.* [2009] describe gas compositions from bubbles collected from the study area and from seeps at 220 m water depth. In both areas, nitrogen concentrations of about 10 vol % were found in bubbles captured by JAGO directly after their release into the water column. Comparison of Figures 13b and 13c shows that the relative amount of methane in the bubble reaching the sea surface is higher relative to the initial amount if the initial bubble contains 10% N_2. Depending on the bubble size distribution and release depth, the difference is between 0.5 to 1%. These relative changes in concentration are enough to transport absolutely more methane to the sea surface.

5.4. Flux Toward the Sea Surface

[44] To evaluate the amount of methane that finally reaches the sea surface and enters the atmosphere, the number of seeps in a certain water depth, the stripping behavior of bubbles with different initial sizes, the bubble size distribution, the gas composition and the activity of the

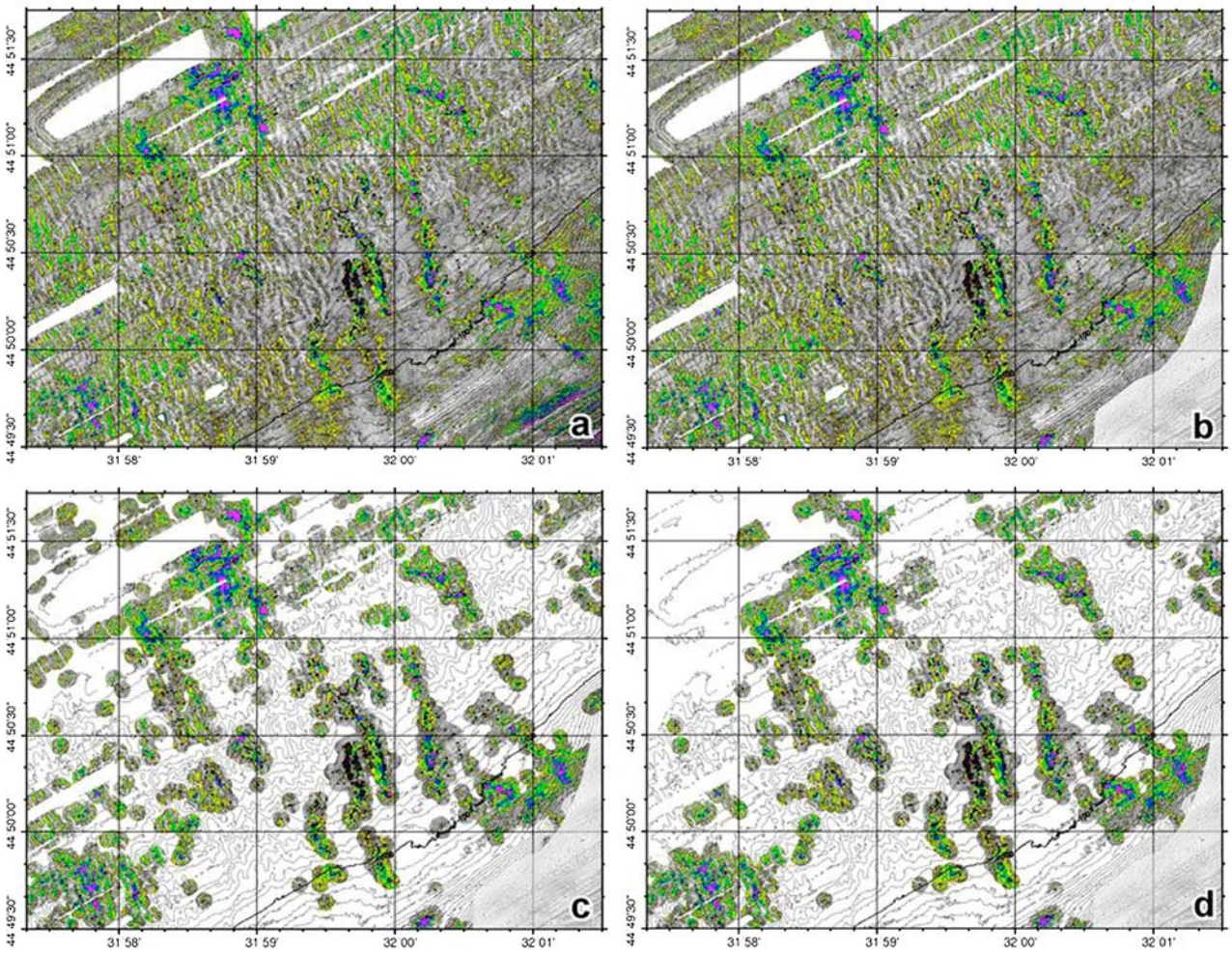

Figure 9. Processing steps that show the cropping of the backscatter map to extract only those areas that are influenced by seepage. (a) The entire mapped area of 21.8 km^2; the number of seeps that would have been calculated with the relation of Figure 8 is 5085. (b) The slope area that was cut off in the SE corner (20.7 km^2 with 4668 seeps calculated). (c) Area after applying the 80 m distance relation given in Figure 10 (9.1 km^2 with calculated 3108 seeps). (d) Map that was used to calculate the final number of 2709 seeps existing in the area (7.3 km^2).

seep have to be considered. For this purpose the area was split in subareas (>73, 73 to 112 in 3 m steps). Based on the backscatter data, the number of seeps per depth interval was estimated and the percentage of methane that reaches the sea surface after stripping was calculated relative to the initial amount (Table 2). Most of the methane is dissolved in the water column. Depending on the initial gas composition and bubble size spectrum, the amount of carbon that is transported to the sea surface from the entire study area is between 20 and 106 kg/d, assuming the seeps are constantly active and release 0.5 mmol/s of gas. Including the temporal variability of seep activity in the calculations (reducing the daily fluxes to only 12%), results in 2.4 to 12.7 kg/d of methane-derived carbon reaching the sea surface (Table 2).

[45] The amount of methane that might enter the atmosphere is greater if all the methane that enters the mixed layer (~15 m water depth, Figure 11) contributes to it. Table 3 gives the amount of methane that is transported into the mixed layer and the amount of methane that dissolves from the rising bubbles within the mixed layer. As this dissolved methane equilibrates with the overlying air, it creates an additional "dissolved" methane flux into the atmosphere (Table 3).

5.5. Comparison to Directly Measured and Hydroacoustically Determined Fluxes

[46] *Schmale et al.* [2005] used a geochemical equilibrator system to directly measure methane concentrations in the study area and calculate the methane fluxes from dissolved methane in seawater (not the bubble flux) toward the atmosphere. Their data clearly show that the dense clusters of seeps in the studied shelf area correlate positively with surface water methane concentrations and methane fluxes into the atmosphere. Surface water methane concentrations above seep clusters were about 2 to 2.5 times higher (up to 7.5 nM) than normal shelf or open water concentrations in the Black Sea (4.5 and 3 nM, respectively). Their flux grid was the base to calculate the flux into the atmosphere from

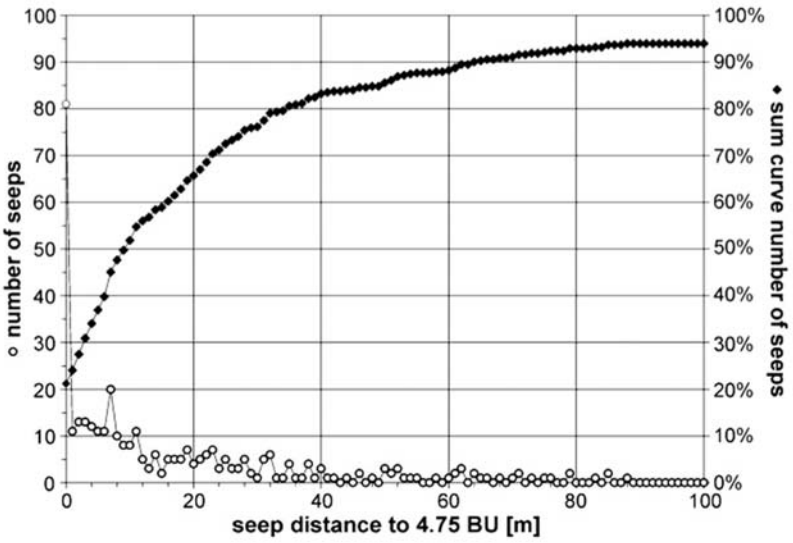

Figure 10. Distance of seeps from backscatter areas with BU values ≥4.75 BU. This value was chosen as threshold for the very high backscatter, only 5% of the seeps plot in these areas (see Figure 6).

the same area as in our study (Figure 15). *Schmale et al.* [2005] used equations from *Liss and Merlivat* [1986, hereinafter LM86] and *Wanninkhof* [1992, hereinafter W92] to calculate the flux of 1030 (LM86) and 2495 (W92) mol/d. The flux calculated after *Wanninkhof* [1992] is in very good agreement with the estimated dissolved methane flux of 2256 to 2366 mol/d for bubble spectrum A, without applying a correction for the temporal variability (Table 3).

[47] *Artemov et al.* [2007] calculate fluxes exclusively based on their single-beam echo sounder data (also used in this study). They detected 902 seeps in the total insonified shelf area (41.2 km^2; down to 140 m water depth) and calculate that each seep releases 101 mmol/min on average (2.47 l/min at STP). This is about 3 times the mean average value yielded by our submersible measurements. They also calculate that 1.52 mol/s of methane (1.17×10^6 m^3/y at STP) are released in total into the water column from the seafloor compared to 1.35 mol/s in this study (that includes 645 seeps from the 902 given by *Artemov et al.* [2007]). These two numbers are in very good agreement for two independently acquired and processed fluxes based on

Table 2. Spatial Extrapolations for Fluxes Into the Water Column and Toward the Sea Surface For Two Initial Bubble Compositions[a]

Release Depth (m)	Number of Seeps	CH_4 Flux Into the Water (mmol/s)		Depth-Related Flux to the Sea Surface as Percent of Initial Amount of CH_4							
				Spectrum A		Spectrum B		Spectrum C		Spectrum D	
		CH_4	$CH_4 + N_2$[b]	CH_4	$CH_4 + N_2$	CH_4	$CH_4 + N_2$	CH_4	$CH_4 + N_2$	CH_4	$CH_4 + N_2$
<73	141	70.5	63.5	6.50	7.13	10.20	10.95	14.67	15.48	19.6	20.47
73–76	507	253.5	228.2	5.29	5.87	8.55	9.27	12.62	13.43	17.3	18.13
76–79	224	112.0	100.8	4.60	5.15	7.58	8.28	11.38	12.19	15.8	16.69
79–82	214	107.0	96.3	3.99	4.52	6.71	7.39	10.25	11.06	14.5	15.35
82–85	316	158.0	142.2	3.36	3.96	5.83	6.59	9.14	10.01	13.2	14.10
85–88	257	128.5	115.7	2.88	3.46	5.11	5.86	8.18	9.05	12.0	12.93
88–91	247	123.5	111.2	2.47	3.02	4.48	5.21	7.31	8.17	10.9	11.84
91–94	171	85.5	77.0	2.11	2.56	3.92	4.55	6.52	7.31	9.9	10.79
94–97	169	84.5	76.1	1.80	2.21	3.42	4.01	5.81	6.56	9.0	9.84
97–100	68	34.0	30.6	1.54	1.91	2.99	3.53	5.16	5.89	8.1	8.97
100–103	161	80.5	72.5	1.32	1.65	2.60	3.11	4.58	5.28	7.3	8.17
103–106	95	47.5	42.8	1.09	1.42	2.22	2.74	4.02	4.73	6.6	7.43
106–109	90	45.0	40.5	0.91	1.23	1.91	2.41	3.54	4.23	5.9	6.75
109–112	49	24.5	22.1	0.76	1.06	1.64	2.12	3.11	3.78	5.3	6.12
Total	2709	1354.5	1219.1								

	Final Flux to the Sea Surface							
	Spectrum A		Spectrum B		Spectrum C		Spectrum D	
	CH_4	$CH_4 + N_2$	CH_4	$CH_4 + N_2$	CH_4	$CH_4 + N_2$	CH_4	$CH_4 + N_2$
CH_4 flux (mmol/s)	45.5	52.5	77.5	86.7	120.2	131.1	172.3	184.3
CH_4 flux (mol/d)	3930	4533	6695	7489	10,385	11,329	14,886	15,921
C flux (kg/d)	47.2	54.4	80.3	89.9	124.6	136.0	178.6	191.0

[a]The two initial bubble compositions used are 100% CH_4 and 90% CH_4 + 10% N_2. A release depth of 70 m was chosen for the dissolution calculations for the area shallower than 73 m. For the deeper depth ranges the center depth value was used (73–76 = 74.5; 76–79 = 77.5; . . .).
[b]Here it is 90% CH_4 and 10% N_2.

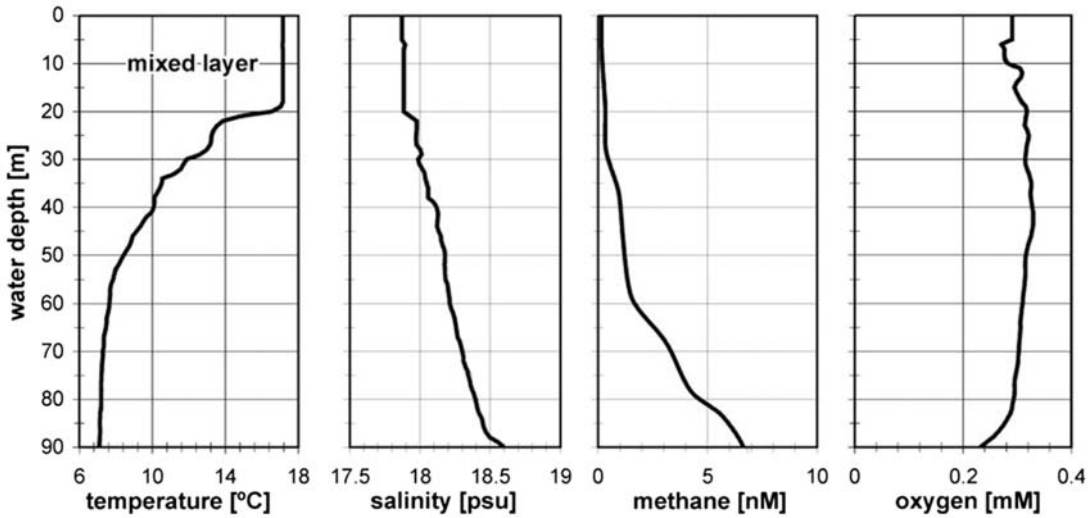

Figure 11. Environmental conditions and concentrations of important geochemical species used for bubble stripping modeling. The mixed layer depth was conservatively set at 15 m water depth based on the temperature profile.

hydroacoustic methods. However, the results for the final flux toward the sea surface and into the atmosphere are different. *Artemov et al.* [2007] used their own bubble dissolution model and calculated that about 26% of the initially released methane reaches the sea surface (0.31×10^6 m^3/y at STP or 403 mmol/s). This is significantly more than our model calculations predict.

5.6. Known Uncertainties

[48] Flux estimates based on extrapolations as described here raise questions about the uncertainties involved and the statistical validity of the results. One uncertainty is caused by the sporadic activity of the seeps [*Greinert*, 2008], and that ship-based echo sounder data used for the correlation between backscatter values and seeps/m2 only capture seeps that were active during the single-beam surveys. To enhance the probability that most of the bubble releasing seeps in the area had actually been discovered, we explicitly used a smaller area (subarea, Figure 5) that showed the densest concentration of seeps and a dense/repeated survey grid, to establish a correlation between backscatter value and seep occurrence.

[49] A second, very common source of uncertainty is the limited observation and monitoring time of the real flux at the seafloor. The assumed flux rate of 0.5 mmol/s (1.17 ml/s in situ, Table 1) is based on real data but may not be a valid and a reliable average for the entire area. The measured volume and mol fluxes of the studied shelf seeps are low (maximum of 0.63 mmol/s; Table 1) compared to in situ fluxes elsewhere, e.g., at the Håkon Mosby Mud Volcano [*Sauter et al.*, 2006], Hydrate Ridge [*Torres et al.*, 2002] or the Batumi seep area in the eastern Black Sea [*Nikolovska et al.*, 2008] (Table 1). It is not surprising that the mol fluxes from these areas are much higher due to the much greater water depth, but also the volume fluxes are 1–2 orders of magnitude higher than those measured. *Dimitrov* [2002a] presents fluxes from the Bulgarian shelf (Table 1) where the lower range limit is nearer to the flux measured in the study area.

[50] Third, it has to be carefully considered whether a correction for the temporal variability has to be applied or not. Applying a correction for temporal variability to the fluxes into the water column (here 12% [*Greinert*, 2008]) significantly decreases the final flux into the atmosphere and mixed layer that does not agree with the independently measured fluxes by *Schmale et al.* [2005]. The most likely reason is the upscaling from the very accurate measurements in a "small" area (2075 m^2) as monitored by the GasQuant system [*Greinert*, 2008] in respect to the entire seep influenced study area of 7.3×10^6 m^2 (Figure 9). The good agreement between the dissolved methane flux determined by *Schmale et al.* [2005] and the amount of methane dissolving in the mixed layer suggest that a correction for the temporal variability is not needed. The high number of seeps identified in the area and the good coverage with the single-beam echo sounder accounted for this temporal variability already. Thus we suggest that the finally calculated number of 2709 seeps is a good estimate of the number of "constantly" active seeps.

6. Conclusions

[51] This paper describes a technique that can be used to estimate the methane flux from a seep area. It has been shown that a combination of hydroacoustic methods (single-beam echo sounder for seep detection, multibeam for backscatter mapping, GasQuant for detecting temporal variability) works well for calculating spatially and temporally corrected methane bubble fluxes from seeps to the sea surface. Applying bubble stripping modeling that takes into account the release depths and bubble size distributions gave a realistic estimate of the flux into the atmosphere. This flux is comparable to independently determined fluxes by single-beam studies (flux into the water column [*Artemov et al.*, 2007]) and is in good agreement to geochemical equilibrator surveys that directly measured the methane flux into the atmosphere [*Schmale et al.*, 2005].

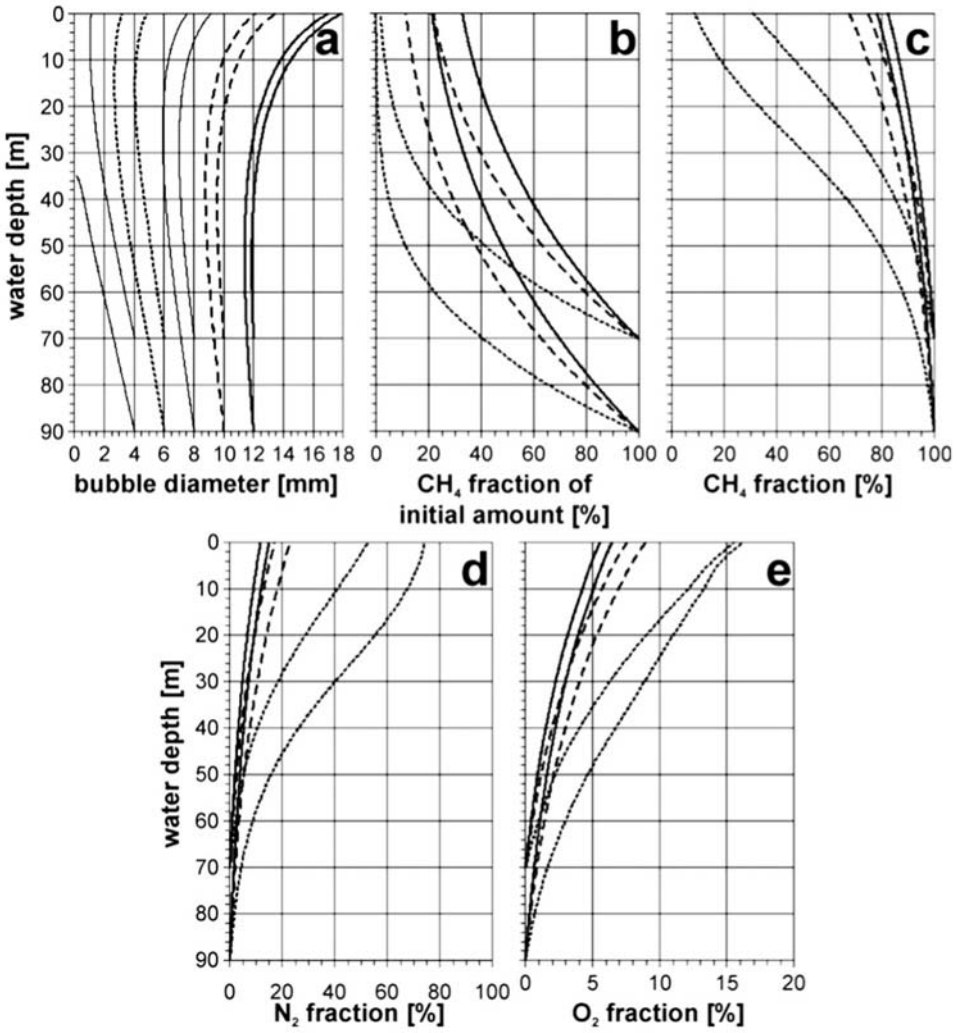

Figure 12. Model runs for the bubble dissolution clearly show that bubble size and release depth have a great impact on the amount of methane that is finally transported to the sea surface. Shown are runs for 70 and 90 m water depth and three different bubble sizes of 6, 10, and 12 mm diameter as dotted, dashed, and solid lines, respectively. (a) The change of bubble size during bubble rise. (b) The percent of methane that is present in the bubble during rise relative to the initial amount (Figure 12b). (d and e) Bubbles strip nitrogen and oxygen from the water and (b and c) methane is dissolved. The stripping effect is greater with smaller bubbles; large bubbles with 12 mm initial diameter transport 22% (from 90 m depth) to 34% (70 m depth) of the initial methane to the atmosphere.

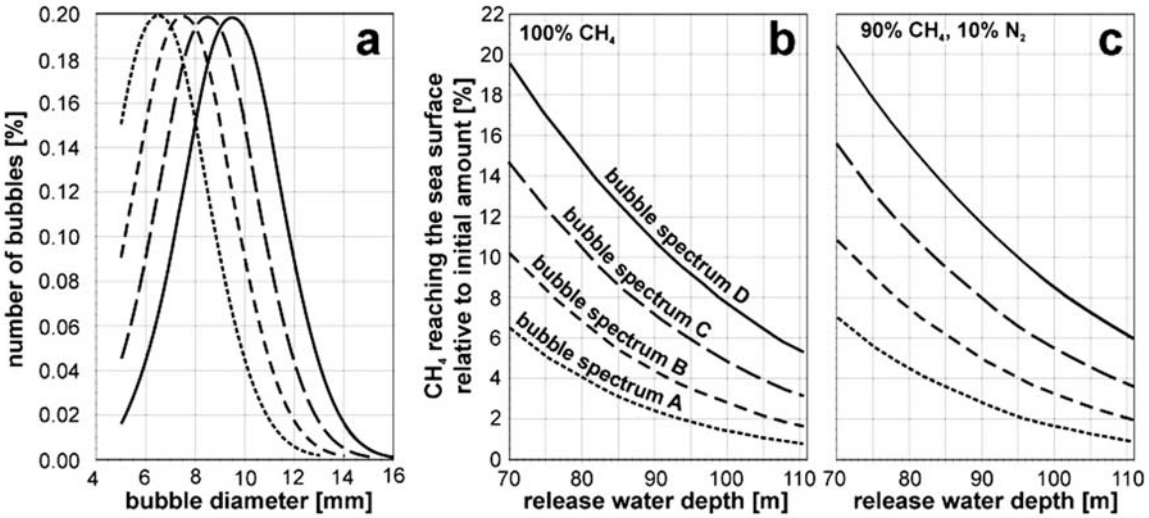

Figure 13. Amount of methane that reaches the sea surface relative to the initially released methane amount. (a) Histogram of four bubble size spectra assuming Gaussian distribution that were used to compute the relative amount of methane in the bubble during its rise. (b) All bubble size spectra had a width value (wv) of 2 mm and varying center values (cv) of 6.5, 7.5, 8.5, and 9.5 mm; f(cv) = EXP($-1cv^2/(2wv^2)$). The bubble size spectrum that most closely matches those observed is spectrum A. The amount of methane that reaches the sea surface for pure methane bubbles (Figure 13b). (c) All bubble size spectra assumed 10 vol % of nitrogen and 90 vol % CH_4. The absolute amount of methane transported toward the sea surface is higher if 10% N_2 are present in the initial bubble (Table 2).

[52] To put the flux obtained for the most realistic bubble spectrum A in perspective, we compare it to methane release by sheep and carbon release from cars. An average "New Zealand" sheep releases about 20 g of methane per day [*Lassey et al.*, 1997; *Murray et al.*, 2001, and references therein]. This means that 3144 to 5519 sheep release the same amount of carbon directly into the atmosphere as the estimated 2709 seeps in the studied area (Table 3; New Zealand has about 40,000,000 sheep). A small modern car releases about 120 g CO_2 per km. Thus a car journey of 1441 to 2530 km would release the same amount of carbon (3930 to 6899 mol/d) as the entire study area.

[53] In conclusion, the data illustrate that the studied seeps with their predominately small bubbles transport a rather limited amount of methane into the atmosphere at their currently low activity. However, the fluxes would rapidly increase with increasing bubble size and decreasing water depth (Table 2). The probability that shallow shelf areas, i.e., of the Arctic, will become a significant source of methane in the future is very high [e.g., *Shakhova et al.*,

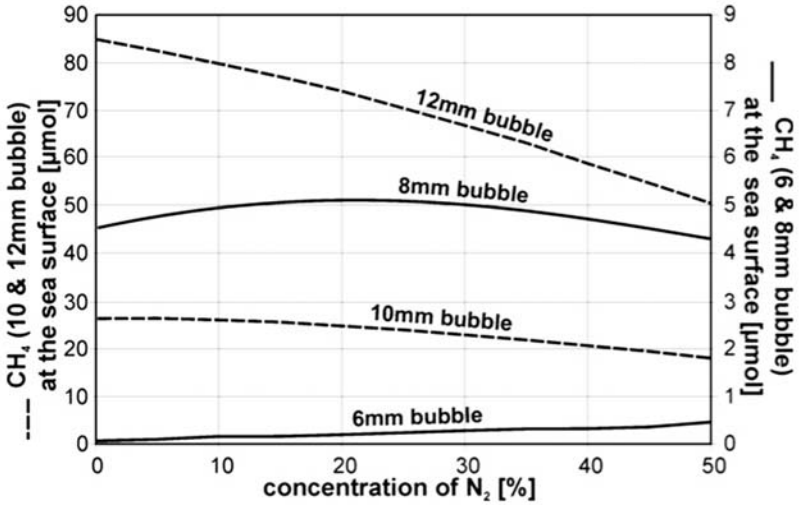

Figure 14. Change of the amount of methane that reaches the sea surface depending on the initial bubble size and the amount of nitrogen (vol %) at release. The release depth for the model runs was 90 m and the environmental conditions are those from Figure 11, the same as for all other model calculations.

Table 3. Final Bubble Fluxes Into the Atmosphere or the Mixed Layer for the Different Bubble Size Spectra A–D[a]

	Spectrum A		Spectrum B		Spectrum C		Spectrum D	
	CH_4	$CH_4 + N_2$[b]	CH_4	$CH_4 + N_2$	CH_4	$CH_4 + N_2$	CH_4	$CH_4 + N_2$[b]
CH_4 flux to the sea surface (mol/d)	3930	4533	6695	7489	10,385	11,329	14,886	15,921
CH_4 flux into the mixed layer (mol/d)	6186	6899	9873	10,742	14,439	15,402	19,647	20,639
CH_4 dissolving in the mixed layer (mol/d)	2256	2366	3178	3253	4054	4072	4761	4719
C flux to the sea surface (kg/d)	47.2	54.4	80.3	89.9	124.6	136.0	178.6	191.0
C flux into the mixed layer (kg/d)	74.2	82.8	118.5	128.9	173.3	184.8	235.8	247.7
Number of New Zealand sheep (20gCH_4/d) releasing the same amount of C	3144–4949	3627–5519	5356–7898	5991–8594	8308–11,551	9063–12,321	11,908–15,717	12,737–16,511
Kilometer to be driven by car (120 g CO_2/km) to release the same amount of C	1441–2268	1662–2530	2455–3620	2746–3939	3808–5294	4154–5647	5458–7204	5838–7568

[a]Here the mixed layer is at 15 m water depth.
[b]Here it is 90% CH_4 and 10% N_2.

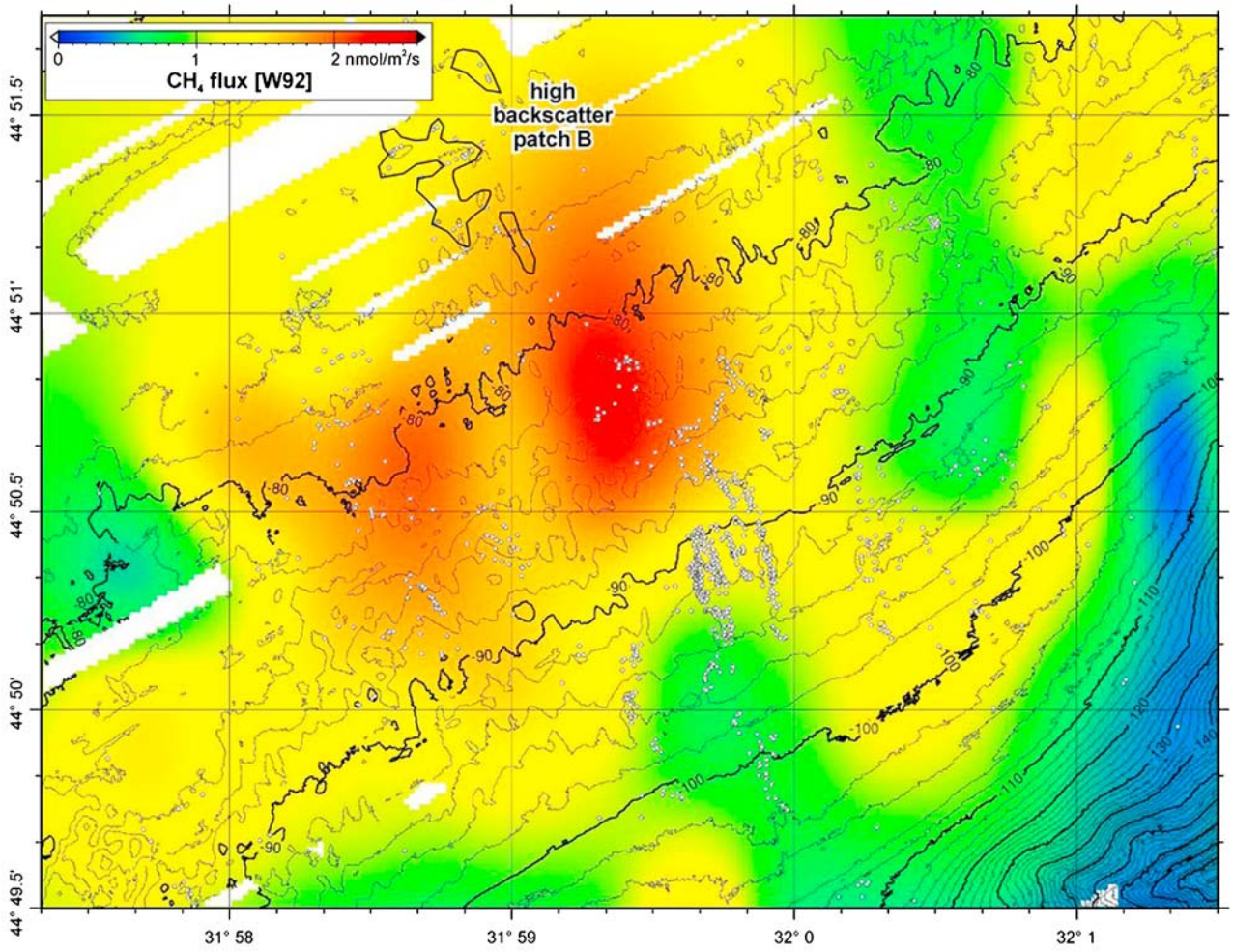

Figure 15. Map of the methane flux from the study area based on data from *Schmale et al.* [2005]. The original grid was resampled to 25 × 25 m, areas for which no backscatter data exist were cut out. The shown values are calculated after *Wanninkhof* [1992]. The miscorrelation between the highest sea surface methane concentrations and the area of the highest seep density or the largest high-backscatter area B (outlined; see also Figure 3) may be due to gridding artifacts, wind-induced drift of sea surface water, and current-induced shifting of bubbles during their rise.

2005; *Shakhova and Semiletov*, 2007; *Semiletov et al.*, 2007] and studies like this may help to design cleverly planned mapping campaigns, direct flux measurements and long-term monitoring stations.

[54] **Acknowledgments.** We would like to thank the crew of RV *Prof. Vodyanitskiy* for their enthusiasm during the cruises in 2003 and 2004. We also thank L3 Communications ELAC Nautik GmbH, Kiel, Germany, for the great support by using the Seabeam 1050 system during the 2 years of mapping. J. Greinert very much appreciated the invitation to the POSEIDON 317–3 cruise by Christian Borowski and Bo Barker Jørgensen (MPI-Bremen, Germany), which provided the opportunity to dive with the submersible JAGO (METROL project). We also thank Yuriy Artemov for supporting us with seep position data. We appreciated the very helpful comments by Andrew Jones and Ray Wood, which helped to clarify the processing steps and make the paper scientifically more focused. We thank both for final, very careful proofreading. Final thanks go to the European Union for financing the CRIMEA (EVK-2-CT-2002-00162) and METROL (EVK-3-CT-2002-00080) projects as well as funding J. Greinert via a Marie Curie grant (MOIF-CT-2005-007436). J. Greinert worked at IFM-GEOMAR during the CRIMEA project.

References

Anon, L. (1991), *Simrad EK500 Scientific Echo Sounder Instruction Manual*, 32 pp., Simrad, Horten, Norway.

Artemov, Y. G. (2006), Software support for investigation of natural methane seeps by hydroacoustic method, *Mor. Ehkol. Zh.*, *5*, 57–71.

Artemov, Y. G., V. N. Egorov, G. G. Polikarpov, and S. B. Gulin (2007), Methane emission to the hydro- an atmosphere by gas bubble streams in the Dieper Paleo-Delta, the Black Sea, *Mor. Ehkol. Zh.*, *6*, 5–26.

Bange, H. W. (2006), Nitrous oxide and methane in European coastal waters, *Estuarine Coastal Shelf Sci.*, *70*, 361–374, doi:10.1016/j.ecss.2006.05.042.

Boetius, A., and E. Suess (2004), Hydrate Ridge: A natural laboratory for the study of microbial life fueled by methane from near-surface gas hydrates, *Chem. Geol.*, *205*, 291–310, doi:10.1016/j.chemgeo.2003.12.034.

Boudreau, B. P., B. S. Gardiner, and B. D. Johnson (2001), Rate of growth of isolated bubbles in sediments with a diagenetic source of methane, *Limnol. Oceanogr.*, *46*, 616–622.

Dimitrov, L. I. (2002a), Contribution to atmospheric methane by natural seepages on the Bulgarian continental shelf, *Cont. Shelf Res.*, *22*, 2429–2442, doi:10.1016/S0278-4343(02)00055-9.

Dimitrov, L. I. (2002b), Mud volcanoes—The most important pathway for degassing deeply buried sediments, *Earth Sci. Rev.*, *59*(1–4), 49–76, doi:10.1016/S0012-8252(02)00069-7.

Egorov, V., U. Luth, C. Luth, and M. B. Gulin (1998), Gas seeps in the submarine Dnieper Canyon, Black Sea: Acoustic, video and trawl data, in *MEGASEEPS Gas Explorations in the Black Sea, Project Report*, edited by U. Luth, C. Luth, and H. Thiel, pp. 11–21, Univ. of Hamburg, Hamburg, Germany.

Egorov, V. N., G. G. Polikarpov, S. B. Gulin, Y. G. Artemov, N. A. Stokozov, and S. K. Kostova (2003), Modern conception about forming-casting and ecological role of methane gas seeps from bottom of the Black Sea, *Mor. Ehkol. Zh.*, *2*, 5–26.

Etiope, G. (2004), New directions: GEM–geologic emissions of methane, the missing source in the atmospheric methane budget, *Atmos. Environ.*, *38*, 3099–3100, doi:10.1016/j.atmosenv.2004.04.002.

Etiope, G., and R. W. Klusman (2002), Geologic emissions of methane to the atmosphere, *Chemosphere*, *49*, 777–789, doi:10.1016/S0045-6535(02)00380-6.

Greinert, J. (2008), Monitoring temporal variability of bubble release at seeps: The hydroacoustic swath system GasQuant, *J. Geophys. Res.*, *113*, C07048, doi:10.1029/2007JC004704.

Greinert, J., and D. F. McGinnis (2009), Single bubble dissolution model—The graphical user interface SiBu-GUI, *Environ. Modell. Software*, *24*, 1012–1013, doi:10.1016/j.envsoft.2008.12.011.

Greinert, J., Y. Artemov, V. Egorov, M. De Batist, and D. McGinnis (2006), 1300-m-high rising bubbles from mud volcanoes at 2080 m in the Black Sea: Hydroacoustic characteristics and temporal variability, *Earth Planet. Sci. Lett.*, *244*, 1–15, doi:10.1016/j.epsl.2006.02.011.

Holzner, C. P., D. F. McGinnis, C. J. Schubert, R. Kipfer, and D. M. Imboden (2008), Noble gas anomalies related to high-intensity methane gas seeps in the Black Sea, *Earth Planet. Sci. Lett.*, *265*, 396–409, doi:10.1016/j.epsl.2007.10.029.

Hornafius, J. S., D. Quigley, and B. P. Luyendyk (1999), The world's most spectacular marine hydrocarbon seeps (Coal Oil Point, Santa Barbara Channel, California): Quantification of emissions, *J. Geophys. Res.*, *104*, 20,703–20,711, doi:10.1029/1999JC900148.

Hovland, M., A. G. Judd, and R. A. Burke (1993), The global flux of methane from shallow submarine sediments, *Chemosphere*, *26*, 559–578, doi:10.1016/0045-6535(93)90442-8.

Judd, A. G. (2004), Natural seabed gas seeps as sources of atmospheric methane, *Environ. Geol.*, *46*, 988–996, doi:10.1007/s00254-004-1083-3.

Kessler, J. D., W. S. Reeburgh, J. Southon, R. Seifert, W. Michaelis, and S. C. Tyler (2006), Basin-wide estimates of the input of methane from seeps and clathrates to the Black Sea, *Earth Planet. Sci. Lett.*, *243*, 366–375, doi:10.1016/j.epsl.2006.01.006.

Kvenvolden, K. A., and B. W. Rogers (2005), Gaia's breath-global methane exhalations, *Mar. Pet. Geol.*, *22*, 579–590, doi:10.1016/j.marpetgeo.2004.08.004.

Lassey, K. R., M. J. Ulyatt, R. J. Martin, C. F. Walker, and I. D. Shelton (1997), Methane emissions measured directly from grazing livestock in New Zealand, *Atmos. Environ.*, *31*, 2905–2914, doi:10.1016/S1352-2310(97)00123-4.

Leifer, I., and I. R. MacDonald (2003), Dynamics of the gas flux from shallow gas hydrate deposits: Interaction between oily hydrate bubbles and the oceanic environment, *Earth Planet. Sci. Lett.*, *210*, 411–424, doi:10.1016/S0012-821X(03)00173-0.

Leifer, I., and R. K. Patro (2002), The bubble mechanism for methane transport from the shallow sea bed to the surface: A review and sensitivity study, *Cont. Shelf Res.*, *22*, 2409–2428, doi:10.1016/S0278-4343(02)00065-1.

Liss, P. S., and L. Merlivat (1986), Air-sea exchange rates: Introduction and synthesis, in *The Role of Air-Sea Exchange in Geochemical Cycling*, edited by P. Buat-Menard, pp. 113–127, Springer, New York.

Luyendyk, B., J. Kennett, and J. F. Clark (2005), Hypothesis for increased atmospheric methane input from hydrocarbon seeps on exposed continental shelves during glacial low sea level, *Mar. Pet. Geol.*, *22*, 591–596, doi:10.1016/j.marpetgeo.2004.08.005.

McGinnis, D. F., J. Greinert, Y. Artemov, S. E. Beaubien, and A. Wuest (2006), Fate of rising methane bubbles in stratified waters: How much methane reaches the atmosphere?, *J. Geophys. Res.*, *111*, C09007, doi:10.1029/2005JC003183.

Michaelis, W., et al. (2002), Microbial reefs in the Black Sea fueled by anaerobic oxidation of methane, *Science*, *297*, 1013–1015, doi:10.1126/science.1072502.

Murray, P. J., E. Gill, S. L. Balsdon, and S. C. Jarvis (2001), A comparison of methane emissions from sheep grazing pastures with different management intensities, *Nutr. Cycling Agroecosyst.*, *60*, 93–97, doi:10.1023/A:1012654928177.

Naudts, L., J. Greinert, Y. Artemov, P. Staelens, J. Poort, P. Van Rensbergen, and M. De Batist (2006), Geological and morphological setting of 2778 methane seeps in the Dnepr paleo-delta, northwestern Black Sea, *Mar. Geol.*, *227*, 177–199, doi:10.1016/j.margeo.2005.10.005.

Naudts, L., J. Greinert, Y. Artemov, S. E. Beaubien, C. Borowski, and M. De Batist (2008), Anomalous sea-floor backscatter patterns in methane venting areas, Dnepr paleo-delta, NW Black Sea, *Mar. Geol.*, *251*, 253–267.

Nikolovska, A., H. Sahling, and G. Bohrmann (2008), Hydroacoustic methodology for detection, localization, and quantification of gas bubbles rising from the seafloor at gas seeps from the eastern Black Sea, *Geochem. Geophys. Geosyst.*, *9*, Q10010, doi:10.1029/2008GC002118.

Oguz, T. (2002), Role of physical processes controlling oxycline and suboxic layer structures in the Black Sea, *Global Biogeochem. Cycles*, *16*(2), 1019, doi:10.1029/2001GB001465.

Sahling, H., et al. (2009), Vodyanitskii mud volcano, Sorokin trough, Black Sea: Geological characterization and quantification of gas bubble streams, *Mar. Pet. Geol.*, *26*, 1799–1811, doi:10.1016/j.marpetgeo.2009.01.010.

Sauter, E. J., S. I. Muyakshin, J.-L. Charlou, S. Schlüter, A. Boetius, K. Jerosch, E. Damm, J.-P. Foucher, and M. Klages (2006), Methane discharge from a deep-sea submarine mud volcano into the upper water column by gas hydrate-coated methane bubbles, *Earth Planet. Sci. Lett.*, *243*, 354–365, doi:10.1016/j.epsl.2006.01.041.

Schmale, O., J. Greinert, and G. Rehder (2005), Methane emission from high-intensity marine gas seeps in the Black Sea into the atmosphere, *Geophys. Res. Lett.*, *32*, L07609, doi:10.1029/2004GL021138.

Schmale, O., S. Beaubian, G. Rehder, J. Greinert, and S. Lombardi (2009), Gas seepage in the Dnepr paleo-delta area (NW-Black Sea) and its regional impact on the water column methane cycle, *J. Mar. Syst.*, doi:10.1016/j.jmarsys.2009.10.003, in press.

Schneider, J., J. Greinert, N. R. Chapman, W. Rabbel, and P. Linke (2009), Acoustic imaging of natural gas bubble ebullition in the North Sea: Sensing the temporal, spatial and activity variability, *Limnol.Oceanogr. Methods*, in press.

Semiletov, I. P., I. I. Pipko, I. Rapina, and N. E. Shakhova (2007), Carbonate chemistry dynamics and carbon dioxide fluxes across the atmosphere-ice-water interfaces in the Arctic Ocean: Pacific sector of the Arctic, *J. Mar. Syst.*, *66*, 204–226, doi:10.1016/j.jmarsys.2006.05.012.

Shakhova, N., and I. Semiletov (2007), Methane release and coastal environment in the east Siberian Arctic shelf, *J. Mar. Syst.*, *66*, 227–243, doi:10.1016/j.jmarsys.2006.06.006.

Shakhova, N., I. Semiletov, and G. Penteleev (2005), The distribution of methane on the Siberian Arctic shelves: Implications for the marine methane cycle, *Geophys. Res. Lett.*, *32*, L09601, doi:10.1029/2005GL022751.

Sommer, S., O. Pfannkuche, P. Linke, R. Luff, J. Greinert, M. Drews, S. Gubsch, M. Pieper, M. Poser, and T. Viergutz (2006), Efficiency of the benthic filter: Biological control of the emission of dissolved methane from sediments containing shallow gas hydrates at Hydrate Ridge, *Global Biogeochem. Cycles*, *20*, GB2019, doi:10.1029/2004GB002389.

Torres, M. E., J. McManus, D. E. Hammond, M. A. de Angelis, K. U. Heeschen, S. L. Colbert, M. D. Tryon, K. M. Brown, and E. Suess (2002), Fluid and chemical Fluxes in and out of sediments hosting methane hydrate deposits on Hydrate Ridge, OR, part I: Hydrological provinces, *Earth Planet. Sci. Lett.*, *201*, 525–540, doi:10.1016/S0012-821X(02)00733-1.

Wanninkhof, R. (1992), Relationship between wind speed and gas exchange over the ocean, *J. Geophys. Res.*, *97*(C5), 7373–7382, doi:10.1029/92JC00188.

Wessel, P., and W. H. F. Smith (1998), New, improved version of generic mapping tools released, *Eos Trans. AGU*, *79*, 579, doi:10.1029/98EO00426.

M. De Batist, J. Greinert, and L. Naudts, Renard Centre of Marine Geology, Ghent University, Krijgslaan 281 s8, B-9000 Ghent, Belgium. (greinert@nioz.nl)

P. Linke and D. F. McGinnis, Leibniz Institute of Marine Science, IFM-GEOMAR, Wischhofstrasse 1-3, D-24148 Kiel, Germany.